



Wildfire-Induced CO Plume Observations From NAST-I During the FIREX-AQ Field Campaign

Daniel K. Zhou , Allen M. Larar, Xu Liu , Anna M. Noe, Glenn S. Diskin, Amber J. Soja, G. Thomas Arnold, and Matthew J. McGill

Abstract—The fire influence on regional to global environments and air quality (FIREX-AQ) field campaign was conducted during August 2019 to investigate the impact of wildfire and biomass smoke on air quality and weather in the continental United States. One of the campaign's scientific objectives was to estimate the composition of emissions from wildfires. Ultraspectrally resolved infrared radiance measurements from aircraft and/or satellite observations contain information on tropospheric carbon monoxide (CO) as well as other trace species present in fire emissions. A methodology for retrieving tropospheric CO from such remotely sensed spectral data has been developed for the National Airborne Sounder Testbed-Interferometer (NAST-I) and is applied herein. Retrievals based on NAST-I measurements are used to demonstrate CO retrieval capability and characterize fire emissions. NAST-I remotely sensed CO from ER-2 flights are evaluated with concurrent *in situ* measurements from the differential absorption carbon monoxide measurements flown on the NASA DC-8 aircraft. Enhanced CO emissions along with plume evolution and transport from the fire ground site locations were captured by moderate vertical and high horizontal resolution observations obtained from the NAST-I IR spectrometer; these were intercompared and verified by the cloud physics lidar and the enhanced MODIS airborne simulator also hosted on the NASA ER-2 aircraft. This study will be beneficial to the science community for studying wildfire-related topics and understanding similar remotely sensed observations from satellites, along with helping to address the broader FIREX-AQ experiment objectives of investigating the impact of fires on air quality and climate.

Index Terms—Air quality, carbon, fires, infrared measurements, remote sensing.

I. INTRODUCTION

CHEMISTRY and composition of smoke from wildfires and agricultural burning are studied to improve our understanding of the relationship between combustion burning and air

Manuscript received July 5, 2020; revised January 11, 2021 and February 10, 2021; accepted February 13, 2021. Date of publication February 19, 2021; date of current version March 17, 2021. This work was supported in part by the NOAA JPSS Program Science Office, NASA Headquarters, and NASA Langley Research Center under the NAST-I Program. (Corresponding author: Daniel K. Zhou.)

Daniel K. Zhou, Allen M. Larar, Xu Liu, Anna M. Noe, and Glenn S. Diskin are with the NASA Langley Research Center, Hampton, VA 23681 USA (e-mail: daniel.k.zhou@nasa.gov; allen.m.larar@nasa.gov; xu.liu-1@nasa.gov; anna.m.noe@nasa.gov; glenn.s.diskin@nasa.gov).

Amber J. Soja is with the NASA Langley Research Center, Hampton, VA 23681 USA, and also with the National Institute of Aerospace, Hampton, VA 23666 USA (e-mail: amber.j.soja@nasa.gov).

G. Thomas Arnold is with the NASA Goddard Space Flight Center, Greenbelt, MD 20771 USA, and also with Science Systems and Applications, Inc., Lanham, MD 20706 USA (e-mail: tom.arnold@nasa.gov).

Matthew J. McGill is with the NASA Goddard Space Flight Center, Greenbelt, MD 20771 USA (e-mail: matthew.j.mcgill@nasa.gov).

Digital Object Identifier 10.1109/JSTARS.2021.3059855

quality, weather, and climate forecasts [1]. The fire influence on regional to global environments and air quality (FIREX-AQ) of August 2019 is the first joint field campaign conducted by NOAA and NASA addressing wildfire emissions and their impact on air quality and climate. It is dedicated to the sampling and characterization of fires and their impact on air quality and weather from the point of trace species emissions [2], [3]. Carbon monoxide (CO) is one of the major pollutants due to combustion; air particles downwind of combustion often show elevated CO resulting from photochemical production [4]. The significance of CO in atmospheric chemistry was recognized long ago when a photochemically driven chain reaction was recognized linking the tropospheric cycles of CO, methane (CH₄), and ozone (O₃) with those of the hydroxyl radical (OH) and hydroperoxyl radical (HO₂) [5]. Tropospheric chemical reactions involving CO extend their influence on air quality and the global climate through accumulation of greenhouse gases. Due to its relatively long lifetime (averaging about 2 months in the atmosphere), CO can be transported a great distance from its original source.

The critical role of satellite observations has been established by providing necessary global and regional observations in order to understand the complex chemistry and transport processes involved in regional air pollution chemistry and its influence on the global environment. In December 1999, the measurement of pollution in the troposphere (MOPITT) instrument was launched aboard the TERRA satellite [6], [7] for space-based measurement of CO and CH₄. In July 2004, the tropospheric emission spectrometer (TES) instrument was launched aboard the Aura satellite to detect tropospheric trace species. One of the objectives of these missions was to monitor global CO distribution [8]. Current ultraspectral infrared sounders on a series of weather satellites, i.e., the atmospheric infrared sounder (AIRS) on Aqua [9], the interferometer atmospheric sounding instrument (IASI) on MetOp [10], and the cross-track infrared sounder (CrIS) on SNPP and JPSS [11] also have the ability to observe trace gases including CO. However, remotely sensed CO from these weather satellites has a lower vertical and horizontal resolution due to the satellite sensor spectral resolutions and spatial footprint sizes, i.e., 12–15 km field-of-view (FOV) or 45 km field-of-regard (FOR).

Similar ultraspectral infrared sounders flown on high-altitude aircraft can provide such measurements with a higher spectral resolution and much smaller footprint size. The National Airborne Sounder Testbed-Interferometer (NAST-I) has been successfully operating on high-altitude aircraft since 1998

[12]–[14]. NAST-I onboard NASA high-altitude research aircraft serves as a spaceborne instrument simulator. NAST-I provides high-spatial linear resolution equal to 13% of the aircraft altitude at nadir (2.6 km FOV on the ground from an ER-2 altitude of 20 km) and 13 FOVs across the aircraft track from 13 NAST-I scan angles (~ 3.4 km apart on the ground from an ER-2 altitude of 20 km). NAST-I spatially scans and provides high-spectral resolution (0.25 cm^{-1}) measurements within the spectral region of $645\text{--}2700 \text{ cm}^{-1}$. It serves as an ideal validation sensor since it measures the same Level-1 data product as many of the sensors it helps to validate (i.e., infrared spectral radiance) and does so at higher spectral and spatial resolutions [15]. NASA Langley Research Center analysis is further benefited by implementing a set of internal algorithms to enable an independent assessment of derived Level-2 products [16]. Airborne field campaigns are generally designed to allow retrieval algorithm enhancements and validation with a set of rich coincidental measurements from other sensors [17]–[19].

In this communication, we demonstrate the ability of NAST-I to monitor tropospheric CO distributions under the extreme concentration conditions associated with wildfires. Different from other airborne field experiments that NAST-I has participated in, FIREX-AQ allowed the aircraft sensors to observe the very unique environment within and surrounding wildfire combustion. NAST-I was part of the scientific payload on board the NASA ER-2 aircraft during FIREX-AQ; it provided the opportunity to observe polluted regions and collect ultraspectral radiance data for demonstrating the NAST-I ability to retrieve elevated trace species (e.g., CO) concentration amounts induced by wildfire combustion. The objectives of this article are to use the data collected during FIREX-AQ to demonstrate NAST-I CO retrieval capability, to intercompare and evaluate NAST-I remotely sensed CO with the differential absorption carbon monoxide measurement (DACOM) *in situ* CO measurements [20], to assess plume correlation between CO and smoke-dust detected by cloud physics lidar (CPL) [21] and the enhanced MODIS airborne simulator (eMAS) [22], and to examine the relationship between the total carbon emission and elevated atmospheric CO amount during fire progression and plume evolution. All evidence leads to the conclusion that an elevated CO plume near a wildfire location was indeed produced by the wildfire combustion and subsequent advection; its evolution and transport were captured by NAST-I measurements during FIREX-AQ. NAST-I data presented in this article were collected under clear-sky conditions. NAST-I CO profile cannot be retrieved under opaque clouds as infrared measurements are not able to penetrate opaque clouds [14]. NAST-I remotely sensed CO profile observations are relevant, and they can contribute to applications such as environment and/or air quality (pollution), atmospheric chemistry and dynamics, and climate monitoring and studies.

The remainder of the article is organized as follows. A brief description of the NAST-I retrieval algorithm and CO retrieval results will be given in Section II. NAST-I CO retrieval intercomparisons and evaluation with DACOM *in situ* CO measurements from the NASA DC-8 aircraft are presented in Section III. Additionally, the CO plume assessments with CPL and eMAS

observations from the NASA ER-2 aircraft along with total carbon emissions from the ground are presented. Conclusions follow in Section IV.

II. CO RETRIEVAL AND ITS PLUME

The intent of the measurement of chemical abundance (such as tropospheric CO) is for monitoring air quality and the initialization of climate process models. Several existing inversion algorithms for retrieving CO from satellite remote sensing measurements in the infrared have been summarized [23]. CO amounts retrieved from satellite thermal infrared data from AIRS, IASI, and CrIS are found elsewhere [24]–[26]. The NAST-I retrieval algorithm was developed, tested, and evaluated mainly for atmospheric temperature and moisture profiles, surface skin temperature and spectral emissivity under cloud-free conditions, or cloud microphysical parameters in cloudy conditions [14], [27]. In the early years of the NAST-I program, field campaigns and algorithm development for retrieving these thermodynamic parameters were mainly for weather satellite sensor applications and associated algorithm development, risk mitigation, and validation [17]–[19]. The NAST-I CO retrieval algorithm was also developed [28] and later improved by the implementation of a surface emissivity retrieval [29]. To summarize the NAST-I retrieval algorithm, Fig. 1 presents a CO retrieval algorithm flowchart showing the three steps of: 1) statistical empirical orthogonal function (EOF) regression; 2) physical simultaneous retrieval; and 3) physical sequential retrieval for CO to further minimize the error and increase vertical sharpening for CO profiles.

We have selected one of the ER-2 flight sorties from August 21, 2019 over the Sheridan wildfire to demonstrate the NAST-I CO retrieval using the step-by-step algorithm described in Fig. 1. The Sheridan wildfire was caused by lightning, started on August 5, 2019, and located at approximately 37 km (23 miles) northwest of Prescott, Arizona in the Chino Valley District (34.80° latitude, -112.85° longitude). As the ER-2 flew over the Sheridan fire location area, the wind was blowing from west to east and the smoke-dust plume was evolving and transporting downstream with the wind from the fire location. Two groups of NAST-I measurements, one from west of the Sheridan fire and the other from the east, are used to demonstrate NAST-I CO retrievals from a relatively clean upwind area (west of the fire) and a polluted downwind area (east of the fire). Fig. 2 plots the CO retrievals from statistical EOF regressions (top panel), physical simultaneous retrievals (middle panel), and physical sequential retrievals (bottom panel). Plots on the left are CO column density; in the middle, CO profiles from a relatively clean area (west of the fire); and on the right, CO profiles from a polluted area (east of the fire). The data plotted in the figure show that enhanced CO physical sequential retrieval is helping to further reduce the noise and increase the profile vertical sharpening.

The NASA ER-2 aircraft was flown over the Sheridan wildfire location back and forth five times in west to east and east to west from August 21 23:26:45 UTC to August 22 00:52:00 UTC to capture the CO plume and its time-evolution. Fig. 3 plots

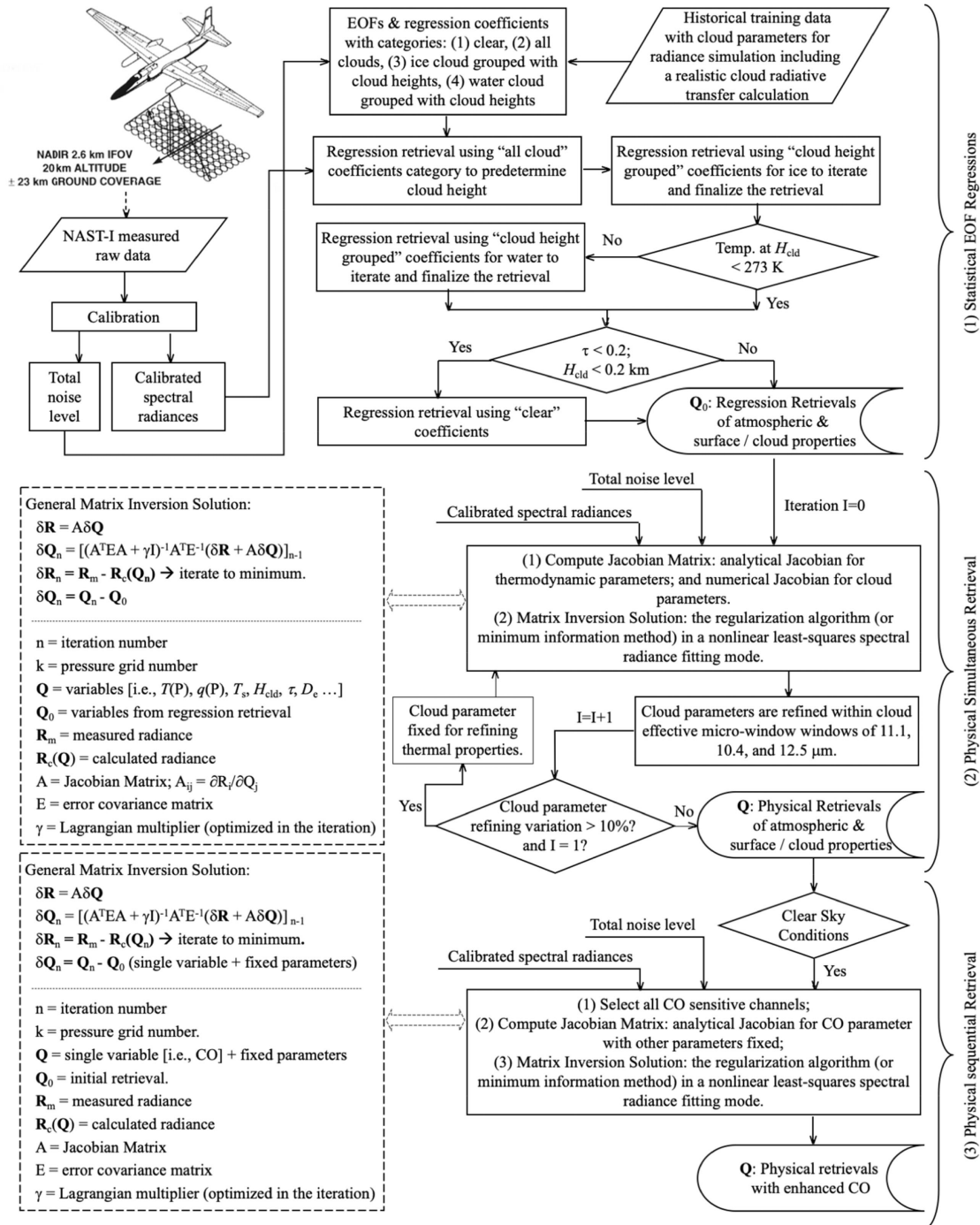


Fig. 1. NAST-I CO retrieval algorithm flowchart, where P is pressure, $T(P)$ is temperature at P , $q(P)$ is water mixing ratio at P , T_s is surface temperature, τ is cloud optical depth, D_e is cloud particle size, and H_{cld} is cloud top height [14], [27]–[29].

the cross sections of the CO vertical profiles near the Sheridan wildfire (about 140 km). Two overpasses are about 70 min apart over the same area showing CO plume evolution and downwind transport from the fire location. Unlike nominal free tropospheric CO, the fire-induced CO plume varies rapidly in space and time, depending on the combination of the specific fire (e.g., fire fuel types) and weather conditions (e.g., wind). Fig. 4 illustrates the 3-D field distribution of CO as observed by NAST-I from the ER-2 flight sortie of August 21, 2019. From these particular

observations, the CO plume went as high as 10–12 km in the atmosphere as we compare CO profiles between upwind nominal tropospheric CO background and the downwind fire-induced CO plume. A high-intensity CO plume was observed at least 70 km downwind (east of the fire location) and ~ 50 km cross wind (i.e., north–south direction). The plume was moving to the area further east of the ER-2 flight region (also shown in Fig. 3). Significant differences in tropospheric CO distributions between upwind and downwind areas are associated with the plume

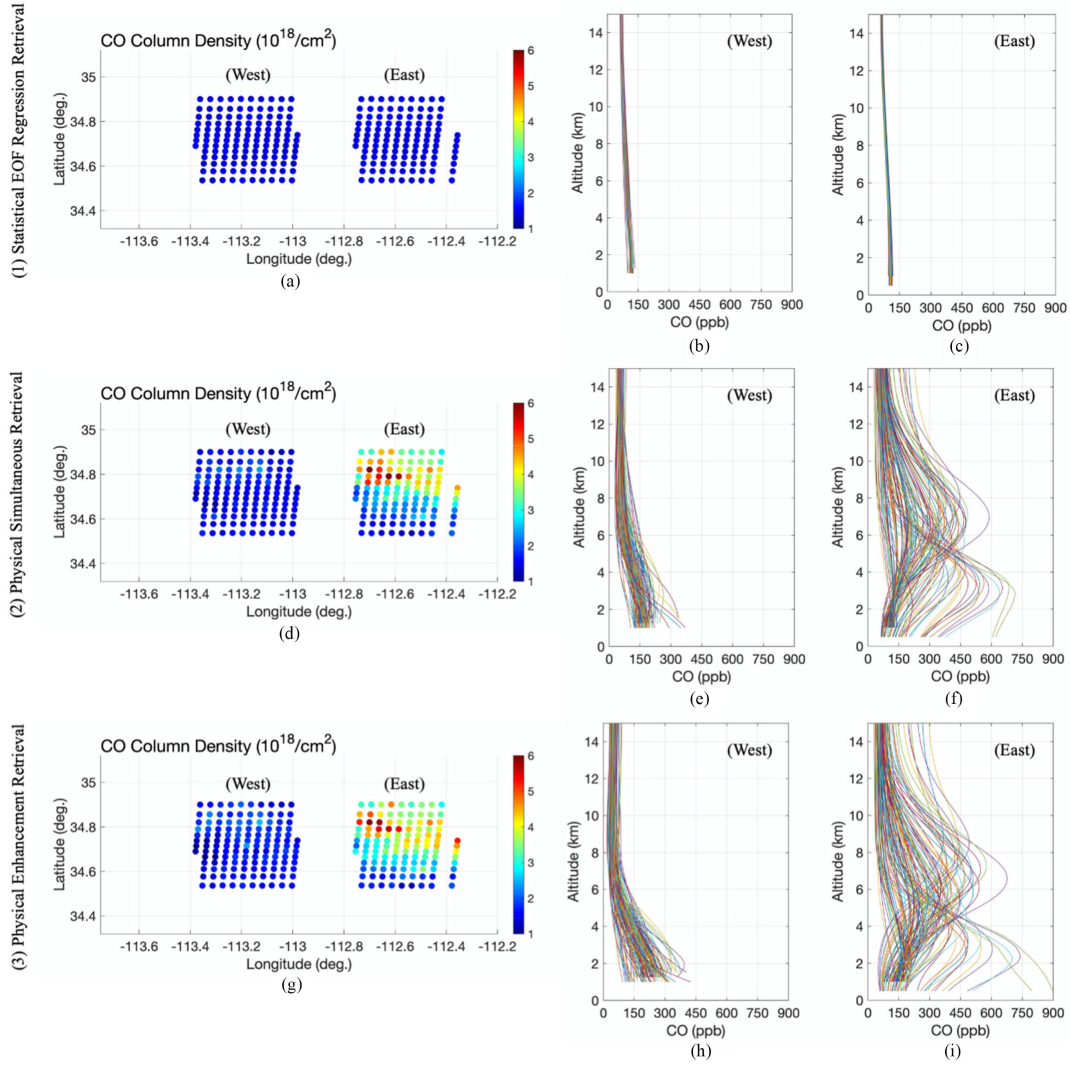


Fig. 2. NAST-I CO retrieval progression through statistical EOF regression (top panel), physical simultaneous retrieval (middle panel), and physical sequential retrieval (bottom panel) from relatively clean (upwind, or west) and polluted (downwind, or east) regions near Sheridan fire on August 21, 2019 (see text).

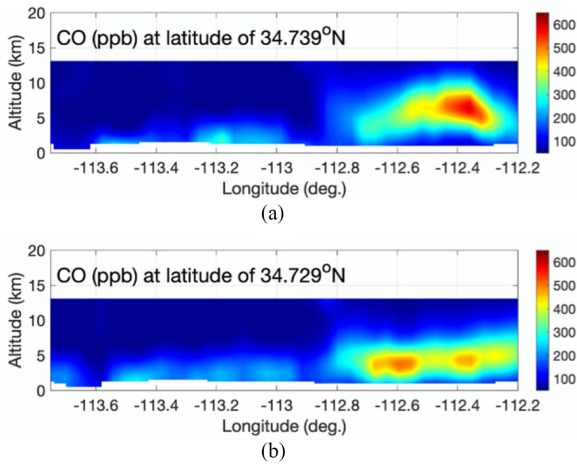


Fig. 3. CO time-evolution shown in its vertical profile cross sections upwind and downwind of the Sheridan fire location (about 140 km) from (a) 23:28:13–23:39:37 UTC of August 21, 2019 to (b) 00:38:35–00:49:24 UTC of August 22, 2019. (a) and (b) are about 70 min apart.

evolution and transport. Small inconsistencies at overlapped geolocations are from time-evolution observed by the ER-2 aircraft being flown back and forth five times, as shown, for example, in Fig. 3. Nevertheless, Fig. 4 gives an overall view of the Sheridan wildfire-induced CO plume in the area captured by NAST-I measurements under biomass burning and weather conditions.

III. EVALUATION AND DISCUSSION

The FIREX-AQ field campaign collected a wealth of coincidental data from numerous remote and *in situ* sensors across multiple aircraft, ground, and satellite observational platforms. Measurements from sensors on aircraft, ground, and satellite are valuable for CO evaluation and science investigation to help characterize different spatial and temporal scales of the plume and associated variability. In this communication, we present a NAST-I CO retrieval intercomparison and evaluation with DACOM CO *in situ* measurements from the NASA DC-8

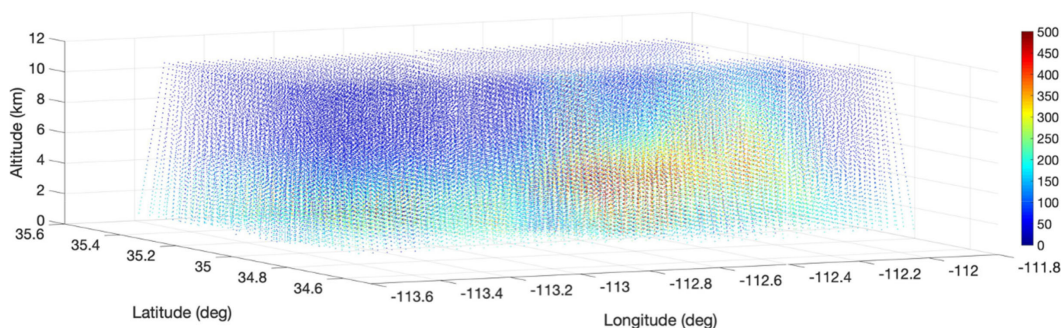


Fig. 4. NAST-I 3-D CO (ppb) distribution shows the plume evolution and transport near the Sheridan fire ground location (34.80° latitude, -112.85° longitude) from August 21, 2019.

aircraft. Moreover, the plume intensity, evolution, and transport are assessed with the smoke-aerosol plume as observed by the CPL and the eMAS from the same ER-2 aircraft. Finally, fire-induced CO amounts in the stratosphere were used to show fire progression linked to total carbon emissions caused by fire combustion.

CO remotely sensed by NAST-I from the ER-2 aircraft can be evaluated with DACOM CO *in situ* measurements from NASA DC-8 aircraft. A few DC-8 sorties were spatially coincident with the ER-2 sorties at the same fire locations but, in general, they had time-lags of a few hours. There was one exception wherein both spatial and temporal coincidence was achieved between the two aircraft, specifically, on August 6, 2019 over the Williams Flats fire that was located at about 11 km (7 miles) southeast of Keller, Washington (47.95° latitude, -118.65° longitude). Fire-induced CO changes rapidly with the nature of the wildfire depending on the fire fuel and weather conditions. Thus, for evaluation purposes, datasets used for intercomparison must be close enough in terms of location and time. It is worth mentioning that *in situ* and remotely sensed observations look at very different parts of the atmosphere, so it is impossible to find a perfect spatial and temporal data match for intercomparison. For this reason, remotely sensed CO from NAST-I and *in situ* CO from DACOM can appear like very different measurements.

Fig. 5 is a flowchart showing how DACOM data are degraded in spatial domain to best match NAST-I spatial resolution within a specific time difference (ΔUTC) of two measurements. This is the methodology currently used in the comparisons presented herein. The quasi-matched DACOM and NAST-I data have $\Delta\text{latitude}$ and $\Delta\text{longitude}$ within $\pm 0.015^\circ$ ($\sim 3 \times 3$ km) and ΔUTC within ± 2 h (or a different ΔUTC window). At the same time, DACOM mean data ($m\text{CO}_D$) are also averaged vertically in altitude dimension. After additional vertical smoothing (i.e., a running average), smCO_D are the vertically smoothed mean within a cube equivalent to NAST-I CO resolution, assuming DACOM data samples collected in the cube can represent the mean of the cube. In reality though, *in situ* data points within the area (or cube) may not be a good representation of what was measured by the remote sensor, especially in a highly nonuniform area such as a wildfire smoke plume. The criteria (i.e., $\Delta\text{latitude}$, $\Delta\text{longitude}$, and vertical smooth factor) for averaged smCO_D to counterpart NAST-I CO data (CO_N) can be adjusted to meet the

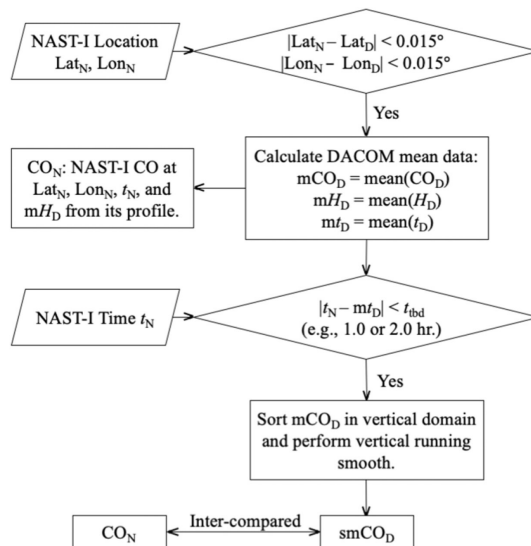


Fig. 5. Flowchart for DACOM *in situ* CO measurement degradation to NAST-I spatial-temporal scales (see text), where H is height and t is time. Subscripts D and N are for DACOM and NAST-I, respectively.

best fitting results between smCO_D and CO_N , where subscripts D and N are for DACOM and NAST-I, respectively. Following the flowchart in Fig. 5, Fig. 6 shows step-by-step averaging of DACOM data to the counterpart NAST-I data. DACOM CO data from Fig. 6(c) (i.e., smCO_D) is then used to compare with CO_N . The methodology for degrading DACOM CO to NAST-I alike is straightforward. The outcome illustrates large differences between CO_D [see Fig. 6(a)] and smCO_D [see Fig. 6(c)]. This shows that DACOM only samples a small part of the extremely heterogeneous environment over which NAST-I observes its FOV mean. Fig. 7(a) [or 7(c), 7(e)] and 7(b) [or 7(d), 7(f)] plot the DACOM and NAST-I data used for intercomparison and where these data are located. Multiple data points at the same altitude are from different locations and/or time. Profiles are not from a single location and time, rather these data points are from the area shown in Fig. 7(b) [or 7(d), 7(f)] during the DC-8 and ER-2 aircraft overlapping period from approximately 18:00 to 23:45 UTC, August 6, 2019. ΔUTC between DACOM and NAST-I for each single data point is less than ± 2 , ± 1 , and ± 0.5 h for the

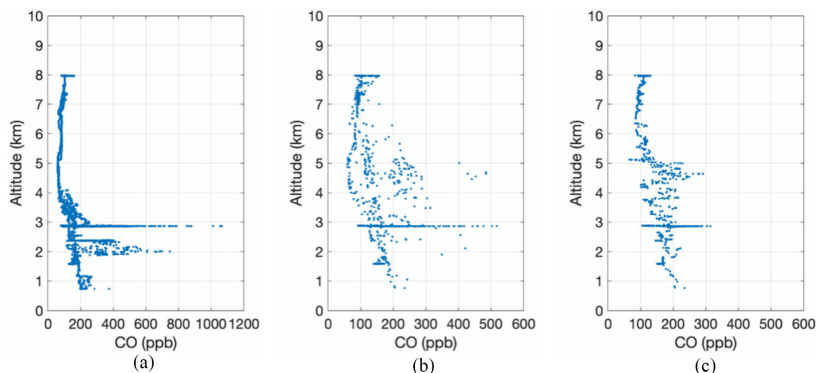


Fig. 6. DACOM *in situ* CO degradation step-by-step to counterpart NAST-I data having Δ latitude and Δ longitude within $\pm 0.015^\circ$, and Δ UTC within ± 2 h: (a) CO_D ; (b) mCO_D ; and (c) smCO_D as described in Fig. 5 flowchart.

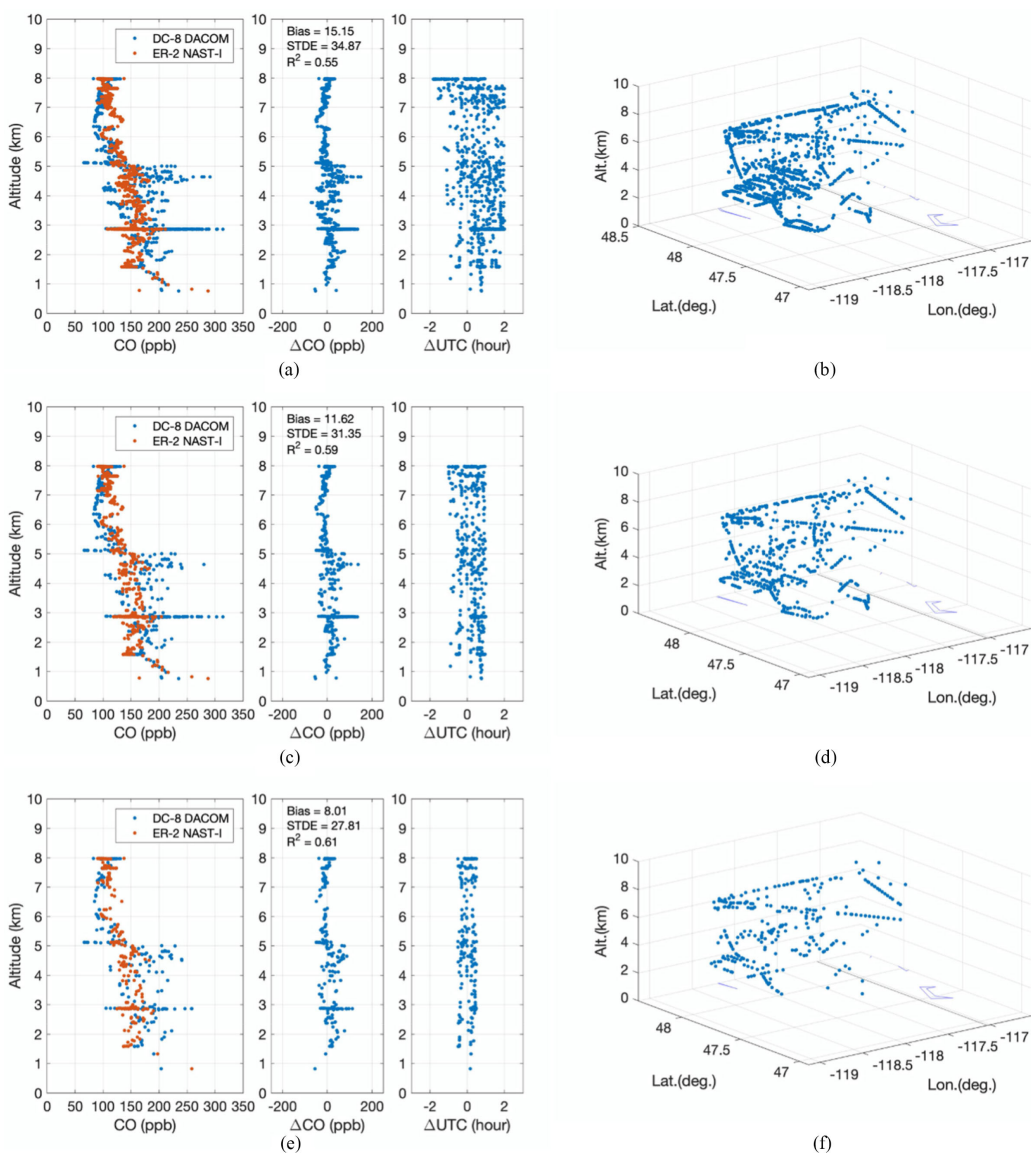


Fig. 7. Intercomparison between DACOM (smCO_D) and NAST-I (CO_N) from August 6, 2019: (a) smCO_D and CO_N comparison with statistical parameters of bias, STDE, and R^2 , and associated Δ UTC is less than ± 2 h and (b) data locations (near Williams Flats fire). (c) and (d) are the same as (a) and (b) but with associated Δ UTC less than ± 1 h; and (e) and (f) are the same as (a) and (b) but with associated Δ UTC less than ± 0.5 h.

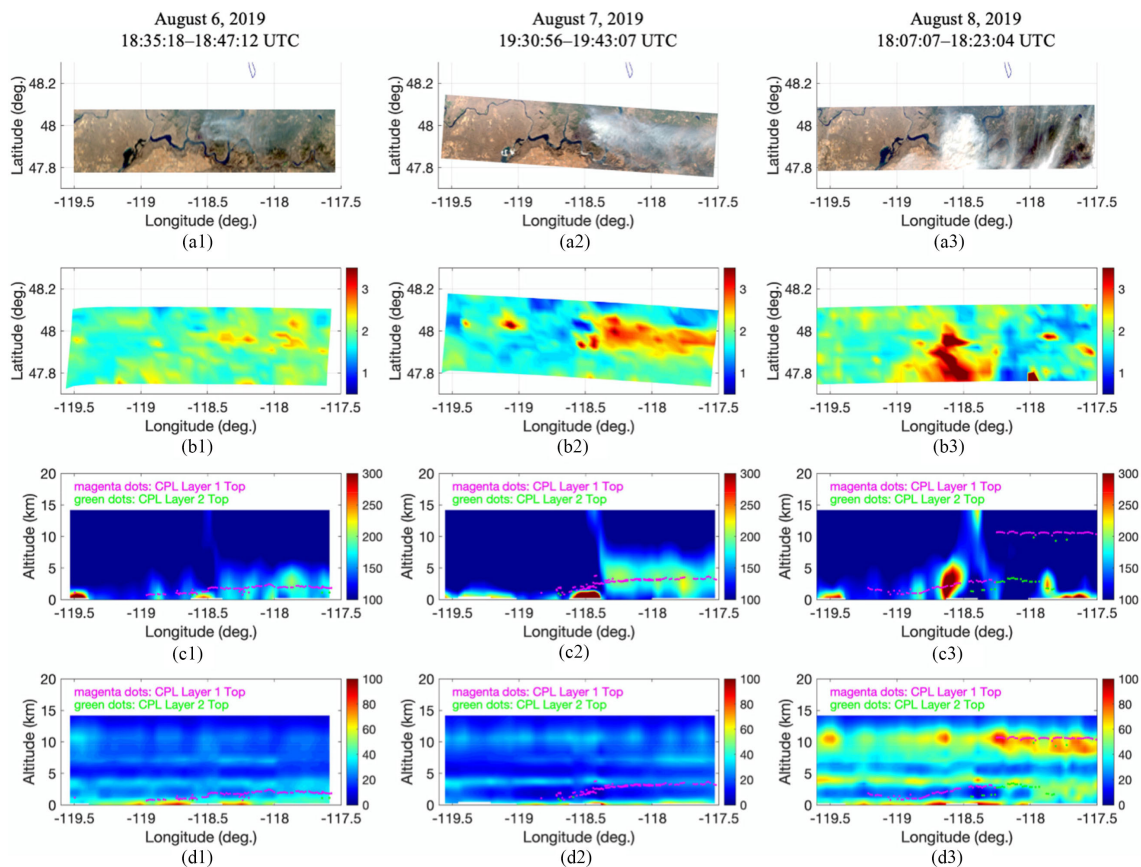


Fig. 8. Williams Flats fire progression from August 6 (left column) to August 7 (middle column), then to August 8 (right column): (a) eMAS true-color imageries; (b) CO column density ($10^{18}/\text{cm}^2$); (c) CO vertical profile (ppb) cross section with CPL layer top; and (d) relative humidity vertical profile (%) cross section with CPL layer top (see text).

upper [see Fig. 7(a) and 7(b)], middle panel [see Fig. 7(c) and 7(d)], and lower panel [see Fig. 7(e) and 7(f)], respectively. The agreement is better with a smaller ΔUTC in terms of the mean bias, standard deviation of difference (STDE), and coefficient of determination R^2 . A positive result is shown in Fig. 7 despite the nature of heavier rapid variation from the wildfire-induced CO plume and the difference between *in situ* and remotely sensed measurements.

The ER-2 aircraft flew to the Williams Flats wildfire location for three consecutive days to observe fire progression. The CO plume intensity, evolution, and transport associated with the fire-produced smoke can be verified by the observations of eMAS and CPL from the same aircraft. The aircraft flew between longitude 117.5°W and 119.6°W with a near constant latitude of 47.9°N , covering 160 km in distance, as shown in Fig. 8. The measurements from both eMAS and CPL confirmed that elevated CO observed by NAST-I is representative and indeed produced by the wildfire. The eMAS is an airborne scanning spectrometer that acquires high spatial resolution (50 m) imagery of cloud (or smoke-aerosol) and surface features. The eMAS has a swath width of about 37 km from the ER-2 flight altitude of 20 km. eMAS imagery from wildfires and its induced smoke-aerosol are observed to identify fire intensity and smoke-aerosol evolution. The Williams Flats fire progression is shown in eMAS measurements. Fig. 8(a)

(the top panel) plots eMAS true-color imagery showing the smoke-aerosol increased from August 6 through 8, 2019, as the measurements taken from ER-2 indicate. It shows the eastward downwind transport during August 6 and 7 before it switched to southern downwind transport on August 8. The NAST-I CO column density and CO nadir vertical profile cross sections are shown in Fig. 8(b) and 8(c), respectively. The CO intensity increased in the downwind transport direction, which is consistent with eMAS smoke-aerosol day-to-day observations.

Smoke-aerosol layers are also measured by CPL. The CPL is a backscatter lidar designed to provide multiwavelength measurements of cirrus, subvisual cirrus, and aerosols with high temporal and spatial resolution (i.e., ~ 200 m in horizontal) along the flight track of the ER-2 aircraft. The CPL-observed cloud and/or aerosol layer top height is plotted on the NAST-I CO vertical profile cross section in Fig. 8(c). The CO plume downwind of the fire location is shown to be correlated with CPL smoke aerosol layer, while the upwind CO is considered as the atmospheric CO nominal background. It can be further identified whether the CPL layer is from aerosol or cloud by the relative humidity retrieved from NAST-I measurements [see Fig. 8(d)]. Relative humidity was low for both August 6 and 7, indicating that there were no clouds present. Therefore, we conclude that the CPL measured layer was an aerosol layer produced by the Williams Flats fire. From August 8, however, the CPL layer

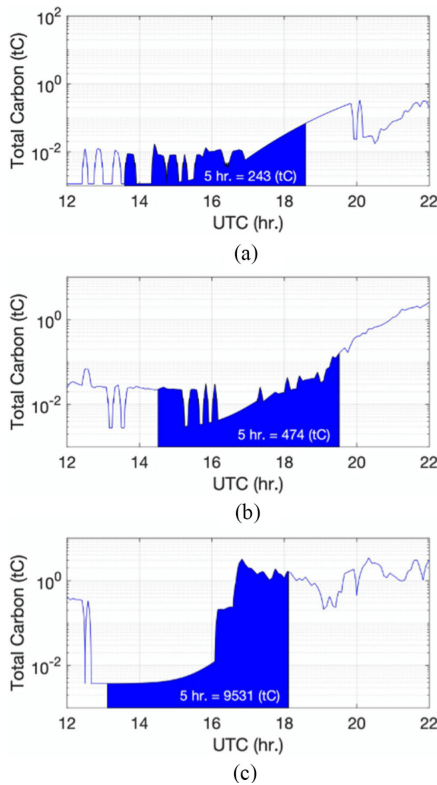


Fig. 9. Total carbon emissions from the Williams Flats fire for (a) August 6, (b) August 7, and (c) August 8, 2019. The area experienced a 5-h total carbon emission prior to the ER-2 observations shown in Fig. 8.

top at ~ 11 km was from cirrus clouds where NAST-I-retrieved relative humidity was about 90%, while a lower layer was from fire-induced smoke-aerosols. It is worth mentioning that CPL has a much higher resolution (200 m) than that of NAST-I (2.6 km). Fire-induced smoke-aerosol is observed to identify smoke-aerosol layer and evolution. Aerosol and CO distributions could vary; and their relationship could be exceedingly complex, even though they are both induced by the same wildfire. It is not studied quantitatively in the scope of this work. However, the correlation of CO and smoke-aerosol plumes induced by the Williams Flats wildfire is recognized. Similar results showing the correlation between wildfire produced CO plumes (observed by NAST-I) and smoke-aerosol plumes (observed by CPL and eMAS) are found in other FIREX-AQ cases such as the Sheridan fire-induced CO plume discussed in Section II.

Another perspective on fire variation can be obtained by examining the total carbon emission from the fire site. Wildfire-induced CO in the troposphere should be linked or proportional to the carbon emission from the fire. Carbon emission from biomass burning can be estimated by a methodology described elsewhere [30]–[32]. Analyses on the carbon emission have been performed for FIREX-AQ including the Williams Flats fire. The total carbon emitted from the Williams Flats fire as a function of time is plotted in Fig. 9. The total carbon amounts from $t - 5$ to t h (where t is ER-2 UTC time shown in Fig. 8) are estimated to be approximately 243, 474, and 9531 tC, from August 6–8,

respectively. We assume that fire-induced CO in the troposphere cumulated in (or moving in and out of) NAST-I observation-space is associated with the carbon emissions from the ground fire during the previous 5 h. This is an irregular assumption as it depends on the weather (i.e., wind), but it should be satisfactory as we are looking at a relative quantity of ground carbon emission versus tropospheric CO amount. The estimation of total carbon emission from these three consecutive days (August 6–8, 2019) shows the Williams Flats fire progression. Tropospheric CO observed by NAST-I shown in Fig. 8(b) and 8(c) is related to the total carbon emission from the Williams Flats fire, reflecting their positive correlation. Tropospheric elevated CO increases as ground total carbon emission increases, which is observed from these three consecutive days. Hence, together with eMAS and CLP observations, we attribute the NAST-I observed elevated tropospheric CO to be fire induced.

IV. CONCLUSION

The FIREX-AQ field campaign with multiple aircraft *in situ* and remotely sensed observations provides the characterization of distributions of chemical species, such as CO, induced by wildfires. This unique dataset is very much desirable in validating CO retrieval algorithms and results with an elevated CO amount. Two wildfire cases from the FIREX-AQ experiment dataset are reported herein, one is from the Sheridan fire and the other is from the Williams Flats fire. Several major summary items and conclusions can be obtained from this work.

- 1) Wildfire-induced CO plumes in the troposphere, in conjunction with their evolution and transport, are readily identified with NAST-I measurements.
- 2) NAST-I retrieval ability is demonstrated showing the contrast between nominal atmospheric background levels and fire-induced elevated CO profiles.
- 3) NAST-I remotely sensed CO is evaluated by favorable intercomparisons with the DACOM *in situ* CO measurements, which show a positive agreement.
- 4) Plume characterization correlation between CO and smoke-dust detected by the CPL and eMAS is assessed and presented a good correspondence.
- 5) Elevated tropospheric CO induced by the wildfire is associated and correlated with the total carbon emission from biomass burning.

First-of-a-kind wildfire-induced CO plume measurements obtained by the NAST-I ultraspectral remote sensor on board the ER-2 suborbital aircraft have shown the intensity and size of wildfire plumes in a high spatial resolution of 2.6 km. Remotely sensed CO from NAST-I is different from *in situ* measured CO as they observe different spatial–temporal parts of the atmosphere, but remotely sensed measurements do have the advantage of giving broader spatial and temporal context by rapidly covering a large field of observation, as shown in Fig. 4. NAST-I onboard the ER-2 suborbital aircraft functions as a spaceborne instrument emulator, demonstrating the ability to monitor CO by an ultraspectral infrared sounder from space with a higher spatial resolution. Data collected by current satellite sounders such as AIRS, CrIS, and IASI can be further investigated in

conjunction with FIREX-AQ datasets to better understand CO retrieval sensitivity and/or ability (e.g., vertical resolution) due to varying instrumental aspects such as FOV size, spectral coverage, spectral resolution, and noise performance. Also, interest in the relationship between CO plume (intensity and size) and total carbon emission from ground biomass burning, and smoke-aerosol distribution from eMAS and CPL measurements, stems in part from the availability of the data and analysis from the FIREX-AQ experiment which will promote further investigation.

NAST-I was successfully operated during all ER-2 flights of the FIREX-AQ experiment (a total of 11 flights and 50+ h of science data collected). NAST-I retrievals (e.g., atmospheric temperature, relative humidity, and CO profiles, also surface skin temperature and CO column density), together with experiment data from other satellite/aircraft/ground measurements and analysis from the FIREX-AQ campaign are available [33] for the science community to study wildfire-related topics as described by the overarching objective of FIREX-AQ experiment [2] and beyond.

ACKNOWLEDGMENT

The authors would like to thank the FIREX-AQ management team, aircraft pilots and crew of NASA ER-2 and DC-8. They would also like to thank L. Rochette of LR Tech, Inc., for his dedicated support of NAST-I instrument upgrade and maintenance, Dr. J. B. Nowak, Dr. J. P. DiGangi, and Dr. H. S. Halliday (now with EPA Research Triangle Park) of NASA Langley Research Center for their contributions to DACOM data acquisition and processing, and Dr. E. B. Wiggins and E. M. Gargulinski of NASA Langley Research Center for their contributions to the total carbon emission calculation. They would also like to thank Dr. M. D. Goldberg of the NOAA JPSS Program Science Office and Dr. J. A. Kaye of the NASA Science Mission Directorate for their continued, enabling support of the NAST-I Program. The NAST-I, DACOM, eMAS, and CPL are part of the Airborne Science Program within the NASA Earth Science Division.

REFERENCES

- [1] P. J. Crutzen, L. E. Heidt, J. P. Krasnec, W. H. Hollock, and W. Seiler, "Biomass burning as a source of atmospheric gases CO, H₂, N₂O, NO, CH₃Cl, and COS," *Nature*, vol. 282, pp. 253–256, Nov. 1979.
- [2] FIREX AQ: Investigating Smoke From Wildfire and Biomass Burning. Accessed: Dec. 15, 2020. [Online]. Available: <https://www.esrl.noaa.gov/csl/projects/firex-aq/>
- [3] D. A. Jaffe *et al.*, "Wildfire and prescribed burning impacts on air quality in the United States," *J. Air Waste Manage. Assoc.*, vol. 70, no. 6, pp. 583–615, Apr. 2020.
- [4] J. Fishman, K. Fakhruzzaman, B. Cros, and D. Nganga, "Identification of widespread pollution in the southern hemisphere deduced from satellite analyses," *Science*, vol. 252, no. 5013, pp. 1693–1696, Jun. 1991.
- [5] H. Levy, II, "Natural atmosphere: Large radical and formaldehyde concentrations predicted," *Science*, vol. 173, no. 3992, pp. 141–143, Jul. 1971.
- [6] L. Pan, J. C. Gille, D. P. Edwards, P. L. Bailey, and C. D. Rodgers, "Retrieval of tropospheric carbon monoxide for the MOPITT experiment," *J. Geophys. Res.*, vol. 103, no. D24, pp. 32277–32290, Dec. 1998.
- [7] M. N. Deeter *et al.*, "Operational carbon monoxide retrieval algorithm and selected results for the MOPITT instrument," *J. Geophys. Res.*, vol. 108, no. D14, Jul. 2003, Art. no. 4399.
- [8] R. Beer, T. A. Glavich, and D. M. Rider, "Tropospheric emission spectrometer for the earth observing system's aura satellite," *Appl. Opt.*, vol. 40, no. 15, pp. 2356–2367, May 2001.
- [9] M. T. Chahine *et al.*, "AIRS: Improving weather forecasting and providing new insights on greenhouse gases," *Bull. Amer. Meteorol. Soc.*, vol. 87, no. 7, pp. 911–926, Jul. 2006.
- [10] F. Hilton *et al.*, "Hyperspectral earth observation from IASI: Five years of accomplishments," *Bull. Amer. Meteor. Soc.*, vol. 93, no. 3, pp. 347–370, Mar. 2012.
- [11] M. Divakarla *et al.*, "The CrMSS EDR algorithm: Characterization, optimization, and validation," *J. Geophys. Res.*, vol. 119, no. 8, pp. 4953–4977, Jan. 2014.
- [12] D. Cousins and W. L. Smith, "National polar-orbiting operational environmental satellite system (NPOESS) airborne sounder testbed-interferometer (NAST-I)," *Proc. SPIE*, vol. 3127, pp. 323–331, Oct. 1997.
- [13] W. L. Smith *et al.*, "NAST-I: Results from revolutionary aircraft sounding spectrometer," *Proc. SPIE*, vol. 3756, pp. 2–8, Oct. 1999.
- [14] D. K. Zhou *et al.*, "Thermodynamic product retrieval methodology for NAST-I and validation," *Appl. Opt.*, vol. 41, no. 33, pp. 6957–6967, Nov. 2002.
- [15] A. M. Larar *et al.*, "IASI spectral radiance validation inter-comparisons: Case study assessment from the JAIVEx field campaign," *Atmos. Chem. Phys.*, vol. 10, no. 2, pp. 441–430, Jan. 2010.
- [16] D. K. Zhou *et al.*, "First Suomi NPP Cal/Val campaign: Inter-comparison of satellite and aircraft sounding retrievals," *IEEE J. Sel. Top. Appl. Earth Observ. Remote Sens.*, vol. 9, no. 9, pp. 4037–4046, Sep. 2016.
- [17] V. Cuomo *et al.*, "The Italian phase of the EAQUATE measurement campaign," *Proc. SPIE*, vol. 5979, pp. 396–409, Nov. 2005.
- [18] J. P. Taylor *et al.*, "EAQUATE: An international experiment for hyperspectral atmospheric sounding validation," *Bull. Amer. Meteorol. Soc.*, vol. 89, no. 2, pp. 203–218, Feb. 2008.
- [19] W. L. Smith, Sr., *et al.*, "Technical note: Evolution, current capabilities, and future advances in satellite ultra-spectral IR sounding," *Atmos. Chem. Phys.*, vol. 9, no. 15, pp. 5563–5574, Mar. 2009.
- [20] G. W. Sachse, G. F. Hill, L. O. Wade, and M. G. Perry, "Fast-response, high-precision carbon monoxide sensor using a tunable diode laser absorption technique," *J. Geophys. Res.*, vol. 92, no. D2, pp. 2071–2081, Feb. 1987.
- [21] M. J. McGill, D. L. Hlavka, W. D. Hart, J. D. Spinhirne, V. S. Scott, and B. Schmid, "The cloud physics lidar: Instrument description and initial measurement results," *Appl. Opt.*, vol. 41, no. 18, pp. 3725–3734, Feb. 2002.
- [22] M. D. King *et al.*, "Airborne scanning spectrometer for remote sensing of cloud, aerosol, water vapor, and surface properties," *J. Atmos. Ocean. Technol.*, vol. 13, no. 4, pp. 777–794, Aug. 1996.
- [23] C. Clerbaux *et al.*, "Retrieval of CO from nadir remote-sensing measurements in the infrared by use of four different inversion algorithms," *Appl. Opt.*, vol. 41, no. 33, pp. 7068–7078, Nov. 2002.
- [24] W. W. McMillan, K. D. Evans, C. D. Barnet, E. S. Maddy, G. W. Sachse, and G. S. Diskin, "Validating the AIRS version 5 CO retrieval with DACOM in situ measurements during INTEx-A and -B," *IEEE Trans. Geosci. Remote Sens.*, vol. 49, no. 7, pp. 2802–2813, Mar. 2011.
- [25] E. De Wachter *et al.*, "Retrieval of MetOp-A/IASI CO profiles and validation with MOZAIC data," *Atmos. Meas. Techn.*, vol. 5, no. 11, pp. 2843–2857, Nov. 2012.
- [26] A. Gambacorta *et al.*, "An experiment using high spectral resolution CrIS measurements for atmospheric trace gases: Carbon monoxide retrieval impact study," *IEEE Geosci. Remote Sens. Lett.*, vol. 11, no. 9, pp. 1639–1643, Sep. 2014.
- [27] D. K. Zhou, W. L. Smith, Sr., X. Liu, A. M. Larar, S. A. Mango, and H.-L. Huang, "Physically retrieving cloud and thermodynamic parameters from ultraspectral IR measurements," *J. Atmos. Sci.*, vol. 64, no. 3, pp. 969–982, Mar. 2007.
- [28] D. K. Zhou, W. L. Smith, X. Liu, J. Li, A. M. Larar, and S. A. Mango, "Tropospheric CO observed with the NAST-I: Retrieval methodology, analyses, and first results," *Appl. Opt.*, vol. 44, no. 15, pp. 3032–3044, May 2005.
- [29] D. K. Zhou *et al.*, "Global land surface emissivity retrieved from satellite ultraspectral IR measurements," *IEEE Trans. Geosci. Remote Sens.*, vol. 49, no. 4, pp. 1277–1290, Jul. 2011.
- [30] W. Seiler and P. J. Crutzen, "Estimates of gross and net fluxes of carbon between the biosphere and atmosphere," *Climate Change*, vol. 2, pp. 207–247, Sep. 1980.
- [31] A. J. Soja *et al.*, "Estimating fire emissions and disparities in boreal Siberia (1998–2002)," *J. Geophys. Res.*, vol. 109, Jul. 2004, Art. no. D14S06.

- [32] R. B. Pierce *et al.*, "Chemical data assimilation estimates of continental U.S. ozone and nitrogen budgets during the intercontinental chemical transport experiment—North America," *J. Geophys. Res.*, vol. 112, Jul. 2007, Art. no. D12S21.
- [33] NOAA/NASA FIREX AQ Campaign Data Archive. Accessed: Dec. 15, 2020. [Online]. Available: <https://asdc.larc.nasa.gov/project/FIREX-AQ>



Daniel K. Zhou received the Ph.D. degree in physics from Utah State University, Logan, UT, USA, in 1992.

He is a Physical Scientist with the Chemistry and Dynamics Branch, Science Directorate, NASA Langley Research Center, Hampton, VA, USA. He has more than 30 years of experience with hyperspectral interferometer remote sensing measurements and data processing. He has worked on numerous programs such as the Cryogenic Infrared Radiance Instrumentation for Shuttle (CIRRIS-1A), National Airborne Sounder Testbed Interferometer (NAST-I),

and the Infrared Atmospheric Sounding Interferometer (IASI), and is currently involved in several remote sensing programs. His experience includes retrieval algorithm development for meteorological and trace gas profile retrieval from remotely sensed infrared measurements, as well as retrieval analyses and validation. His recent research interests include deriving global land surface emissivity spectra, temperatures, and soil moisture from satellite infrared measurements in support of earth observations and climate studies.

Dr. Zhou was the recipient of numerous awards including the NASA Exceptional Achievement Medal.



Allen M. Larar received the Ph.D. degree in atmospheric and space sciences from the University of Michigan, Ann Arbor, MI, USA, in 1993.

He is currently an Associate Director for Research and Mission Science with Science Directorate, NASA Langley Research Center, Hampton, VA, USA. He has more than 25 years of experience of advancing passive remote sensing measurement capabilities. He was the Principal Investigator of the Tropospheric Trace Species Sensing-Fabry-Perot Interferometer (TTSS-FPI) Instrument Incubator Program, successfully completed in 2006, that developed an imaging Fabry-Perot interferometer system, mitigating risks for future geostationary-based measurement of tropospheric ozone. He is currently involved in several remote sensing programs, developing or employing advanced Michelson and Fabry-Perot interferometer systems on ground-, aircraft-, and space-based platforms. His research interests include the remote sensing of thermodynamic state and trace species composition, and he has had extensive involvement in most aspects regarding the development and implementation of advanced passive remote sensing technology for earth atmosphere measurement applications.



Xu Liu received the Ph.D. degree in physical chemistry from the University of Denver, Denver, CO, USA, in 1989.

He is currently a Physical Scientist with the Chemistry and Dynamics Branch, Science Directorate, NASA Langley Research Center, Hampton, VA, USA. He has developed algorithms for radiometric calibration, instrument line shape characterization, fast radiative transfer models, and atmospheric parameter retrievals for various instruments ranging from microwave to visible spectral range. He has

served as a member on various government teams and performed collaborated work with international partners on remote sensing. He has developed a superfast principal-component-based radiative transfer model, which has been successfully applied to hyperspectral sensors such as National Airborne Sounder Testbed Interferometer (NAST-I), Infrared Atmospheric Sounding Interferometer (IASI), Atmospheric InfraRed Sounder (AIRS), Cross-track Infrared Sounder (CrIS), and the Climate Absolute Radiance and Refractivity Observatory (CLARREO).

Dr. Liu was the recipient of numerous awards such as the National Science Foundation Antarctic Service Award, NASA Superior Accomplishment Award, NASA Performance Award, NASA inventions and contributions board awards, and NASA Exceptional Achievement Medal.



Anna M. Noe received the A.A.S. degree in electronics engineering technology and the A.S. degree in science from Thomas Nelson Community College, Hampton, VA, USA, in 1992. She graduated from the NASA Langley apprentice program specializing in electrooptics, in 1994.

She is a Lead Technician for the Remote Sensing Branch, Engineering Directorate, NASA Langley Research Center, Hampton, VA, USA. She has 31 years experience in remote sensing instrument development, test, and integration. She has worked on many projects including the National Airborne Sounder Testbed Interferometer (NAST-I), and is currently involved in several remote sensing programs.

Ms. Noe was the recipient of numerous awards including the NASA Exceptional Achievement Medal and the NASA Exceptional Service Medal.



Glenn S. Diskin received the Ph.D. degree in mechanical and aerospace engineering from Princeton University, Princeton, NJ, USA, in 1997.

He is a Senior Research Scientist with the Chemistry and Dynamics Branch, Science Directorate, NASA Langley Research Center, Hampton, VA, USA. He has more than 35 years' experience making optical measurements in the atmosphere and a variety of ground-based test facilities. He is the Principal Investigator for the DACOM and DLH airborne instruments, and has participated in dozens of airborne

field campaigns, making *in situ* measurements of CO, CO₂, CH₄, N₂O, and H₂O.

Dr. Diskin was the recipient of numerous awards including the NASA Exceptional Technology Achievement Medal.



Amber J. Soja received the Ph.D. degree in environmental sciences from the University of Virginia, Charlottesville, VA, USA, in January 2004.

She is currently an Associate Research Fellow with the National Institute of Aerospace and is resident in the Climate Science and Chemistry and Dynamics Branches of Atmospheric Sciences, NASA Langley Research Center, Hampton, VA, USA. She has 25 years of research experience in using remotely sensed and GIS data to explore the interactions between fire regimes, biomass fuels, land cover, and the atmosphere. She has taken part in and led numerous interdisciplinary, national, and international field campaigns that investigated satellite-defined fire behavior and emissions, and the feedbacks between fire, the biosphere, weather and climate, primarily in remote Siberia (e.g., FireBear, INTEX-A, INTEX-B, TexAQS, ARCTAS, and FIREX-AQ). She was also an Associate Manager with the NASA Applied Sciences Programs Wildland Fire and Disaster. She holds one of the core papers comprising the research front in boreal forest fires and climate change according to *ScienceWatch.com*.

Dr. Soja is currently a member of the International Association of Wildland Fire Board of Directors and a Co-Chair for the Diversity and Inclusivity Committee.



G. Thomas Arnold received the B.S. degree in meteorology, in 1981 and the M.S. degree in atmospheric science from the University of Wyoming, Laramie, WY, USA, in 1986.

He is currently a Chief Research Analyst with Science Systems and Applications Corp and has collaborated with the Climate and Radiation Laboratory, NASA Goddard Space Flight Center, Greenbelt, MD, USA, since 1984. His research interests include aircraft and satellite-based remote sensing of clouds and aerosols, specializing in data analysis via data

visualization, data management, scientific software design, and radiometric instrument calibration.

Matthew J. McGill received the Ph.D. degree in atmospheric science from the University of Michigan, Ann Arbor, MI, USA, in 1996.

He is a Research Scientist with NASA's Goddard Space Flight Center, Greenbelt, MD, USA, with 20+ years' experience developing lidar instrumentation. He is the Principal Investigator for the Cloud Physics Lidar (CPL) instrument and other airborne and spaceborne sensors devoted to the study of clouds and aerosols in the earth's atmosphere.